Variational Neural Network Embedded with Reduced-Order Digital Twins for Online Probabilistic Structural Damage Quantification

Jiaqi Xu * and Xuan Zhou[†]
Beihang University, Beijing, 100191, People's Republic of China

Marco Giglio[‡] and Claudio Sbarufatti[§]
Polytechnic University of Milan, Milan, 20156, Italy

Leiting Dong[¶]
Beihang University, Beijing, 100191, People's Republic of China

Quantifying structural damage using online monitoring data is crucial for condition-based maintenance to ensure aviation safety. However, most data-driven methods hardly utilize accumulated domain knowledge, making it difficult to address parameter variability across different structures due to manufacturing as well as compromising result interpretability. To address these challenges, this study proposes a physics-decoded variational neural network for structural damage quantification and model parameter calibration. The innovation of this method lies in seamlessly integrating a reduced-order digital twin containing damage states and influencing parameters as a decoder within the variational neural network and training a data-driven physical feature extraction model using the variational inference. This architecture enables the training of a data-driven physical feature extraction model using variational inference, facilitating individualized, real-time structural damage quantification and parameter calibration across an entire fleet, while accounting for uncertainties. Validation on typical damaged aeronautical panels demonstrates that the proposed method accurately predicts structural damage states and quantifies associated uncertainties, thereby ensuring high interpretability and accuracy. This approach is expected to be integrated into the airframe digital twin framework to enable condition-based maintenance across a fleet.

*Ph.D. Candidate, School of Aeronautic Science and Engineering; Also affiliated with Tianmushan Laboratory, 310023 Hangzhou, People's Republic of China.

[†]Postdoctoral Fellow, School of Aeronautic Science and Engineering; Also affiliated with Tianmushan Laboratory, 310023 Hangzhou, People's Republic of China; Corresponding author: zhoux@buaa.edu.cn

[‡]Professor, Department of Mechanical Engineering.

[§]Associate Professor, Department of Mechanical Engineering.

[¶]Professor & Chairman of School Council, School of Aeronautic Science and Engineering; Also affiliated with Tianmushan Laboratory, 310023 Hangzhou, People's Republic of China; Corresponding author: ltdong@buaa.edu.cn.

Nomenclature

a	=	crack length
$\mathcal{D}$	=	domain
E	=	Young's modulus
$\mathbb{E}$	=	expectation
$\mathcal{L}$	=	loss function
$\mathcal{M}$	=	full-order model
$\mathcal{M}^r$	=	reduced-order digital twin
$\mathcal{M}^\theta$	=	physical feature extraction model
p, q	=	distribution
$\mathbb{R}$	=	real number set
R	=	stress ratio
t	=	thickness
u	=	node displacement
ur	=	node rotation
$\mathbf{x}$	=	sensor detected signal
$\hat{\mathbf{x}}$	=	reconstruction signal
$\mathbf{z}$	=	physical features
μ	=	weight of the constraint mode
θ	=	parameters of the physical feature extraction model
ϕ	=	parameters of the variational distribution
Λ	=	influencing parameters

Subscripts

p	=	panel skin
panel	=	helicopter panel
s	=	panel stringer

Superscripts

c	=	boundary constraint
exp	=	experiment
g	=	geometric dimension
m	=	material property
meas	=	measurement

norm = normalization

sim = simulation

I. Introduction

STRUCTURAL damage poses a serious threat to aircraft flight safety and may lead to fatal accidents [1]. And damage tolerance is critical in maintaining the structural integrity of aircraft, allowing components to serve with damage, provided the damage state and its implications on airframe safety are well understood. With recent advances in sensor technology, structural health monitoring (SHM) has garnered considerable attention. SHM relies on an integrated sensor network [2, 3] to collect various signals (e.g., strain, temperature, vibration) that are used to detect, localize, and quantify damage within the structure [4]. This capability enables continuous monitoring of structural health and facilitates the estimation of remaining useful life (RUL), thereby supporting both the sustainment of structural integrity and the dynamic scheduling of inspection and maintenance for aeronautical structures [5, 6].

In recent years, data-driven SHM methods have been widely studied [7–14]. These methods directly establish mapping relationships between detected signals and damage states based on their correlations, making them a popular choice for SHM applications due to their straightforward implementation [15–17]. However, purely data-driven approaches inherently lack the incorporation of physical mechanisms, which can result in limited interpretability of damage quantification outcomes [18]. Furthermore, factors such as geometry, material properties, and boundary constraints significantly influence structural damage quantification, yet these are aspects that data-driven methods often struggle to address. This limitation undermines the robustness of the models and reduces their effectiveness in supporting informed decision-making.

To alleviate the shortage of the pure data-driven method, some researchers have explored the integration of physical mechanisms into these models, which can be broadly categorized into three kinds of approaches [19]. The first involves generating representative datasets for data-driven methods guided inherently by physical mechanisms [20–23]. The second incorporates weak additive loss functions into data-driven methods, consisting of the residuals of physical equations and boundary constraints [24–27]. The third forcibly encodes known physical mechanisms into the core architecture of data-driven models to enhance resilience against data sparsity and improve model generalization [28–30].

Decades of research in aeronautical structural integrity have generated substantial domain knowledge. Physics-based models, developed through methods such as the Finite Element Method, enable the prediction of responses in both intact and damaged structures. To leverage this knowledge for structural damage quantification, researchers have investigated several of the aforementioned approaches [31–35]. For instance, Zhang et al. [36] extended neural network inputs and loss function by integrating finite element simulation. Wang et al. [37] combined structural dynamics equations with feature extraction neural networks to achieve deterministic predictions of structural damage. However, in

complex aeronautical structures, the measured responses of damaged components are influenced by the parameters of physics-based models and various uncertainties—factors that current research has yet to adequately address.

Given these challenges, reduced-order digital twins, developed through model reduction techniques, offer a promising solution, as they account for parameter influences and uncertainties while enabling real-time prediction of responses in damaged structures [38–42]. Therefore, integrating physics-based digital twins with the data-driven methods for damage quantification seems beneficial, provided that two challenges can be addressed. First, effectively integrating these influencing factors into the damage quantification process and accurately assessing their specific effects on a given structure remains challenging. This integration is essential for ensuring that damage quantification results are interpreted with precision. Second, the inherent uncertainties in both the influencing factors and the detected signals must be quantified during the online stage to ensure that the results are robust. Addressing these uncertainties is critical for achieving reliable damage quantification.

In this study, the physics-decoded variational neural network (PDVNN) is proposed for online structural damage quantification. The PDVNN integrates a physics-based reduced-order digital twin, which encapsulates both damage states and influencing parameters, into the variational neural network as a decoder. By explicitly representing the damage state and influencing parameters as physical features, the model ensures that physical knowledge relevant to structural damage is embedded within the quantification process. With this approach, structural damage states and influencing parameters can be identified based on detected signals. Furthermore, the use of variational inference allows for the quantification of associated uncertainties. The method is validated on a set of aluminum helicopter panels, demonstrating that the proposed PDVNN achieves higher accuracy and interpretability in structural damage quantification compared to existing data-driven methods.

The remainder of this paper is organized as follows. Section II details the proposed physics-decoded variational neural network and its integration into the structural damage quantification framework. Section III presents the validation of the method on an aeronautical panel, including the experimental setup, numerical model, and comparison methods. Section IV compares and discusses the results, emphasizing the advantages of the proposed approach in damage quantification and parameter calibration. Finally, Section V offers concluding remarks and potential future directions.

II. Development of the Physics-Decoded Variational Neural Network for Structural Damage Quantification

This section details the development of the proposed PDVNN and its application to structural damage quantification, as illustrated in Fig. 1. Section II.A examines the physical mechanisms underlying the responses of intact and damaged structures, along with their influencing factors, which serve as the foundation for developing a physics-based reduced-order digital twin for predicting the response of damaged structures, discussed in Section II.B. Section II.C introduces the integration of the reduced-order digital twin with a data-driven physical feature extraction model, resulting

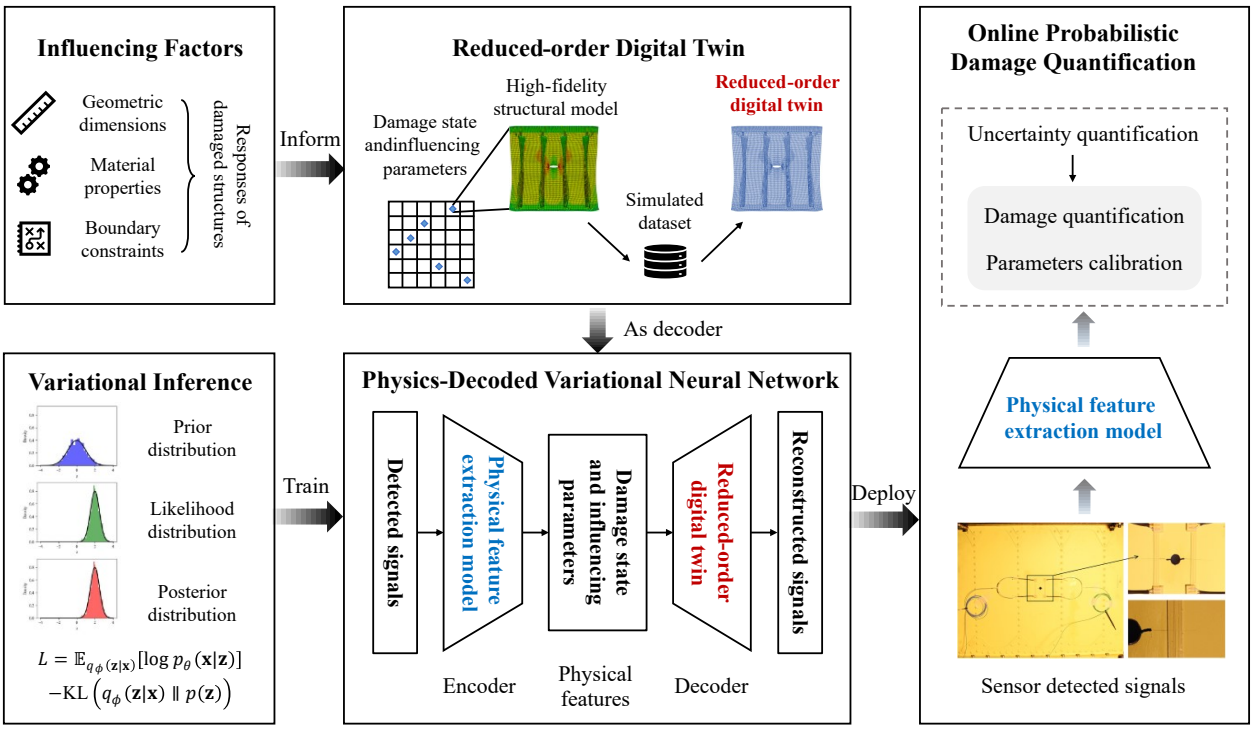

Fig. 1 Flowchart of embedding physics-based digital twin into the variational neural network.

in the formation of the PDVNN. The training of this PDVNN using variational inference is then described in Section II.D. Finally, Section II.E, presents the framework for online structural damage quantification using the PDVNN, which facilitates the quantification of structural damage states and the calibration of digital twin parameters based on detected signals, while accounting for uncertainties. This approach enables individualized damage quantification for identical or similar structures from different sources, such as multiple structures within a fleet.

A. Factors Affecting the Response of Intact and Damaged Structures

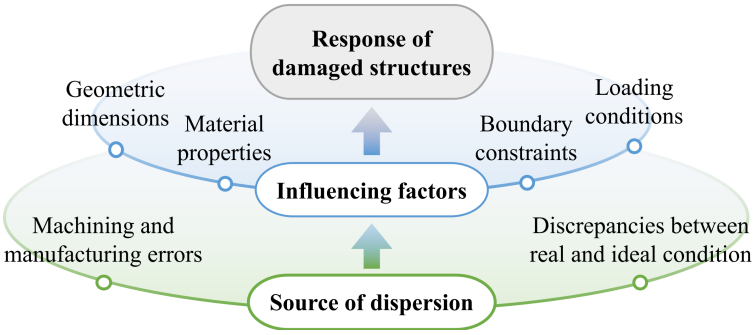

Fig. 2 Source of dispersion and influencing factors in the responses of intact and damaged structures.

In the context of structural damage quantification, domain knowledge includes an understanding of how a structure responds to external loads across different damage states. While physics-based models can simulate structural behavior,

their accuracy is highly dependent on the precise setting of model parameters. As depicted in Fig. 2, two primary sources contribute to variability in these parameters. The first source stems from the inherent variability introduced during the manufacturing stage, where machining and manufacturing errors lead to inconsistencies in geometric dimensions and material properties across different batches and equipment. The second source arises from discrepancies between the real load conditions and boundary constraints encountered during service and the ideal conditions assumed in the simulation model [16].

In structural digital twins that model the response of damaged structures, uncertainties are represented through influencing parameters, denoted as:

$$\boldsymbol{\Lambda} = [\boldsymbol{\Lambda}^g, \boldsymbol{\Lambda}^m, \boldsymbol{\Lambda}^c] \tag{1}$$

where $\boldsymbol{\Lambda}$ is the set of the influencing parameters, with $\boldsymbol{\Lambda}^g$ represents geometric dimensions, $\boldsymbol{\Lambda}^m$ denotes material properties, and $\boldsymbol{\Lambda}^c$ corresponds to boundary constraints.

B. Constructing the Reduced-order Digital Twin Based on Physical Mechanisms

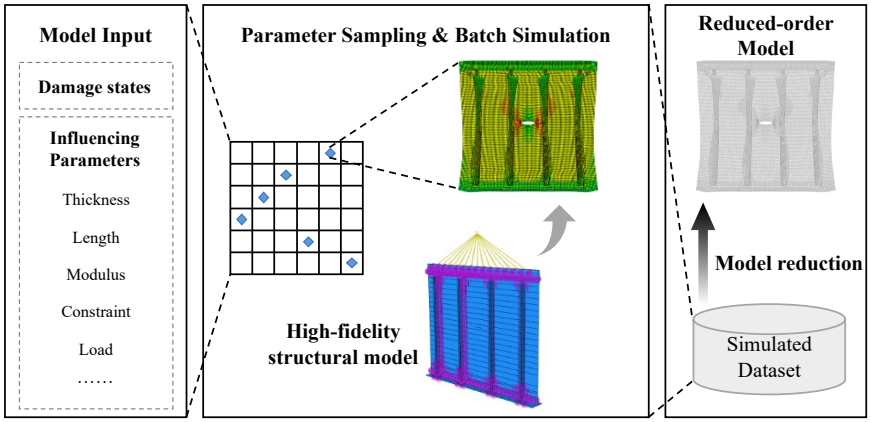

Fig. 3 Flowchart of constructing the reduced-order digital twin.

As illustrated in Fig. 3, the construction of the reduced-order digital twin involves three key steps: parameter sampling, batch simulation, and model training.

First, the influencing parameters of the damaged structures are identified, and sampling is performed within the parameter space to encompass all possible states and variations of these parameters. This process generates a sufficient number of sample points for subsequent batch simulation, with each sample point representing a distinct set of parameters for the simulation model.

Next, these sampled parameters are fed into the full-order simulation model $\mathcal{M}$ to perform the batch simulation, typically using Monte Carlo Simulation (MCS). The structural responses at the sensor network locations are extracted from the simulation output and combined with the corresponding input parameters to form a simulated dataset $\mathcal{D}^{\text{sim}}$ as:

$$\mathcal{D}^{\text{sim}} = \left\{\mathbf{a}^{\text{sim}}, \mathbf{\Lambda}^{\text{sim}}, \mathbf{x}^{\text{sim}}\right\} \tag{2}$$

where $\mathbf{a}^{\text{sim}}$, $\mathbf{\Lambda}^{\text{sim}}$ and $\mathbf{x}^{\text{sim}}$ represent the simulated damage state parameters, influencing parameters, and sensor detected signals, respectively.

Finally, construct a reduced-order digital twin, denoted as $\mathcal{M}^r$, is trained to establish the relationship between the damage states/parameters and the detected signals. This reduced-order model (ROM) effectively serves as an alternative to the full-order simulation model $\mathcal{M}$. In this model, the input consists of the structural damage state $\mathbf{a}$ and the influencing parameters $\mathbf{\Lambda}$, while the output corresponds to the sensor-detected signal $\mathbf{x}$. The ROM can be expressed as:

$$\mathbf{x} = \mathcal{M}^r(\boldsymbol{a}, \mathbf{\Lambda}) \tag{3}$$

It is important to note that the reduced-order digital twin can be constructed using various machine learning methods, such as neural networks [43, 44] and Gaussian process regression [45]. When the model's inputs and outputs are complex, deep learning techniques may be necessary. For instance, convolutional neural networks [46] can be employed for image-type inputs; recurrent neural networks [47] for time-series inputs; and graph neural networks [48] for graph-type inputs. In cases where the digital twin is complex and contains multiple ROMs, a co-simulation approach, such as the functional module interface [49], may be required to integrate these models effectively.

C. Fusing the Physics-Based and Data-Driven Model into the Physics-Decoded Variational Neural Network

Based on the trained reduced-order digital twin model, the PDVNN is constructed as depicted in Fig. 4 (a). The left part of the architecture represents the data-driven physical feature extraction model $\mathcal{M}^\theta$, parameterized by θ, which takes the detected signals $\mathbf{x}$ as input and outputs the latent variables. The middle part represents the physical features, $\mathbf{z} = [\mathbf{a}, \mathbf{\Lambda}]$, where $\mathbf{a}$ is the damage state parameters and $\mathbf{\Lambda}$ is the influencing parameters. These latent variables are probabilistically modeled with the mean $\boldsymbol{\mu}(\mathbf{z})$ and standard deviation $\boldsymbol{\sigma}(\mathbf{z})$. The right part of the PDVNN consists of the reduced-order digital twin, which uses the sampled latent variables as input to reconstruct the sensor signals $\hat{\mathbf{x}}$ as output.

This architecture shares similarities with the classical VAE model, as shown in Fig. 4 (b). However, there are two key differences that enable the PDVNN to perform damage quantification and parameter calibration which is unachievable with VAE. First, the decoder in the PDVNN is replaced by the reduced-order digital twin developed in Section II.B, allowing for the reconstruction of detected signals in a physically meaningful manner. Second, with the digital twin serving as the decoder, the damage state parameters $\mathbf{a}$ and influencing parameters $\mathbf{\Lambda}$ in the PDVNN are explicitly treated as physical features, whereas in a VAE, the latent variables lack physical meaning.

As a result, when the model is properly trained, the damage state and influencing parameters can be probabilistically

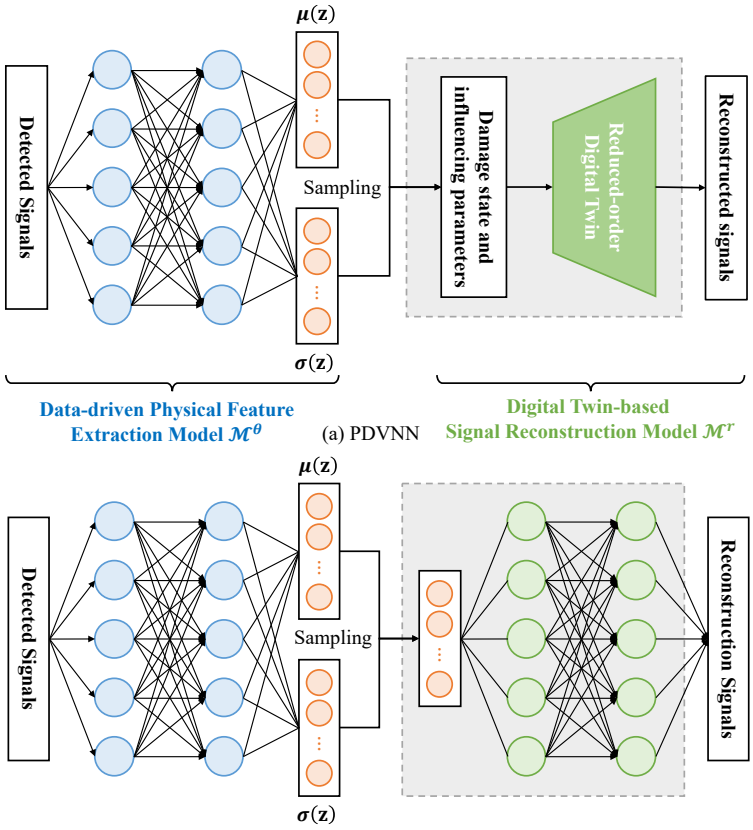

Fig. 4 Architectures of (a) Proposed PDVNN and (b) Classical Variational Autoencoder (VAE).

quantified, providing their mean and variance based on the detected signals as input. Additionally, the signals can be reconstructed using the digital twin. The method for training this model is introduced in the next subsection.

D. Training the Physics-Decoded Variational Neural Network Based on Variational Inference

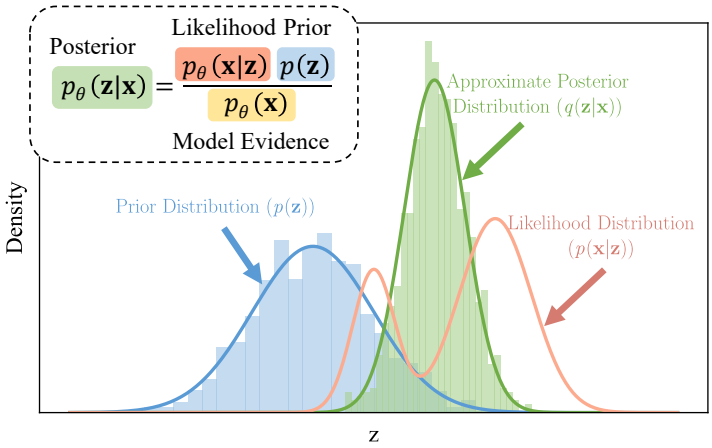

Fig. 5 Approximate Bayesian inference.

As discussed in Section II.A, the response of a damaged structure is influenced by various factors, making it difficult for the ROM to achieve accurate deterministic predictions, especially when the parameters are biased. Consequently, the quantification of uncertainties in the damage state and related parameters becomes crucial. In this subsection, the variational inference method within a Bayesian framework [50] is employed to train the PDVNN, enabling the estimation of uncertainties in both damage states and influencing parameters.

In the PDVNN, the physical features $\mathbf{z}$ are modeled as a probabilistic distribution $p(\mathbf{z})$, rather than a deterministic estimate. Given the detected signal $\mathbf{x}$ in the training dataset, the posterior distribution $p_\theta(\mathbf{z} \mid \mathbf{x})$ can be estimated using Bayes' theorem as shown in Fig. 5:

$$p_\theta(\mathbf{z}|\mathbf{x}) = \frac{p_\theta(\mathbf{x}|\mathbf{z})p(\mathbf{z})}{p_\theta(\mathbf{x})} \tag{4}$$

where $p_\theta(\mathbf{x}|\mathbf{z})$ is the likelihood, $p(\mathbf{z})$ is the prior distribution of the physical features $\mathbf{z}$ and the $p_\theta(\mathbf{x})$ is prior distribution of the detected signal $\mathbf{x}$, also known as the model evidence. However, the true posterior $p_\theta(\mathbf{z}|\mathbf{x})$ is generally intractable due to the complexity of the model. To overcome this, the variational inference introduces a variational distribution $q_\phi(\mathbf{z}|\mathbf{x})$, parameterized by ϕ, to approximate the true posterior. The objective is to minimize the Kullback-Leibler (KL) divergence between the approximate posterior $q_\phi(\mathbf{z}|\mathbf{x})$ and the true posterior $p_\theta(\mathbf{z}|\mathbf{x})$. However, directly minimizing this divergence is difficult because $p_\theta(\mathbf{z}|\mathbf{x})$ involves the marginal likelihood $p_\theta\mathbf{z}$, which is also intractable.

Instead, the PDVNN optimizes the Evidence Lower Bound (ELBO), which can be expressed as:

$$\log p_\theta(\mathbf{x}) \geq \mathbb{E}_{q_\phi(\mathbf{z}|\mathbf{x})}\left[\log p_\theta(\mathbf{x}|\mathbf{z})\right] - \mathrm{KL}\left(q_\phi(\mathbf{z}|\mathbf{x})\|p(\mathbf{z})\right) \tag{5}$$

where the first term $\mathbb{E}_{q_\phi(\mathbf{z}|\mathbf{x})}\left[\log p_\theta(\mathbf{x}|\mathbf{z})\right]$ represents the expected log-likelihood of the data under the variational posterior, commonly referred to as the mean-square error (MSE) loss in traditional neural networks [51], and $\mathrm{KL}\left(q_\phi(\mathbf{z}|\mathbf{x})\|p(\mathbf{z})\right)$ is the KL divergence between the variational posterior $q_\phi(\mathbf{z}|\mathbf{x})$ and the prior $p(\mathbf{z})$.

By maximizing the ELBO, the loss function $\mathcal{L}$ of the PDVNN can be represented as:

$$\mathcal{L} = \mathbb{E}_{q_\phi(\mathbf{z}|\mathbf{x})}\left[\log p_\theta(\mathbf{x}|\mathbf{z})\right] - \mathrm{KL}\left(q_\phi(\mathbf{z}|\mathbf{x})\|p(\mathbf{z})\right) \tag{6}$$

In this manner, the PDVNN simultaneously learns the parameters of the inference model and the posterior distribution $q_\phi(\mathbf{z}|\mathbf{x})$ in a probabilistic framework. Since the variational inference in the PDVNN is analogous to that in the VAE, further details can be found in [52].

With the loss function defined as in Eq. 6, the PDVNN model can be trained. However, in practical scenarios, noise is often present in the detected signals, which can affect the model's robustness. To mitigate this, noise is added to the simulated signals to form the hypothesized noisy signal:

$$\mathbf{x}^{\text{noise}} = \mathbf{x}^{\text{sim}} + \boldsymbol{\varepsilon}^{\text{meas}} \tag{7}$$

where $\boldsymbol{\varepsilon}^{\text{meas}} \sim \mathcal{N}(\mathbf{0}, \boldsymbol{\sigma}_\varepsilon)$ and $\mathcal{N}$ represents a normal distribution. The standard deviation $\boldsymbol{\sigma}_\varepsilon$ is determined by the noise level of the SHM sensors. The model is then trained using the hypothesized noisy signal.

The complete PDVNN algorithm is formulated, with its pseudocode outlined in Algorithm 1.

E. Framework for Structural Damage Quantification and Parameter Calibration Based on the Proposed Algorithm

With the proposed PDVNN, we present the framework for structural damage prediction and parameter calibration, as illustrated in Fig. 6. This framework comprises both offline and online stages.

In the offline stage, a reduced-order digital twin is developed to solve the structural response of the damaged structure using the simulated dataset. The digital twin is then integrated with an initialized physical feature extraction $\mathcal{M}^\theta$ to form the PDVNN. During the training process, the digital twin guides the $\mathcal{M}^\theta$ to extract physical features (the damage states and influencing parameters) through variational inference.

In the online stage, sensor-measured data obtained from physical entities is fed into the feature extraction model In the online stage, the detected signals obtained from the structures are fed into the physical feature extraction model

Algorithm 1 Physics-Decoded Variational Neural Network (PDVNN) for structural damage quantification and parameter calibration

Input: Simulated dataset $\mathcal{D}^{\text{sim}} = \left\{\mathbf{a}^{\text{sim}}, \mathbf{\Lambda}^{\text{sim}}, \mathbf{x}^{\text{sim}}\right\}$.

Output: Physical feature extraction model $\mathcal{M}^{\theta}$.

1. Concatenate the damage state $\mathbf{a}$ and influencing parameters $\mathbf{\Lambda}$ into the physical features $\mathbf{z} = [\mathbf{a}, \mathbf{\Lambda}]$;
2. Define the architecture of the physical feature extraction model $\mathcal{M}^{\theta}$ based on the number of detected signals n_x and latent variables n_z;
3. Construct the reduced-order digital twin $\mathcal{M}^{r}$ with the physical features $\mathbf{z}$ as input and the detected signals $\mathbf{x}$ as output;
4. Add noise in the simulated signals to obtain a hypothesized noisy signal $\mathbf{x}^{\text{noise}}$ as in Eq. 7;
5. Integrate the $\mathcal{M}^{\theta}$ and pretraind $\mathcal{M}^{r}$ into a PDVNN model, and train the model with the $\mathbf{x}^{\text{noise}}$ as dataset and the loss function $\mathcal{L}$ in Eq. 6;
6. Derive the trained $\mathcal{M}^{\theta}$ for structural damage quantification and parameter calibration.

Return: M_{θ}.

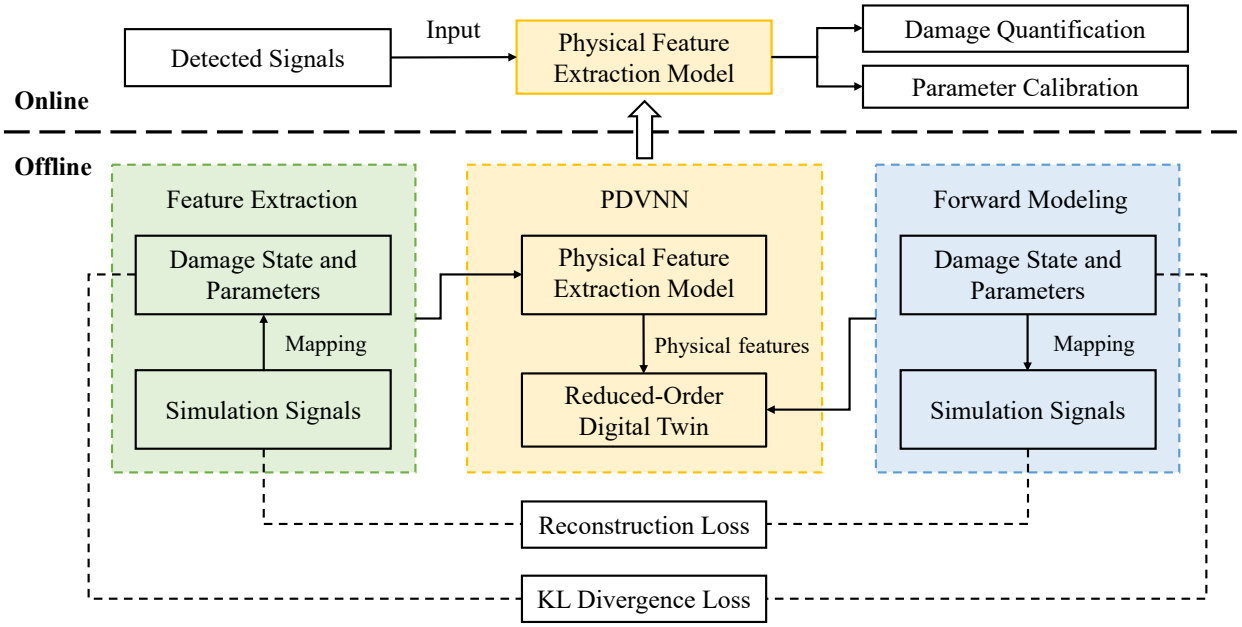

Fig. 6 Structural damage quantification and parameter calibration with the proposed Physics-Decoded Variational Neural Network.

developed in the offline stage. This process enables structural damage quantification and parameter calibration in a probabilistic manner, ensuring both accuracy and interpretability.

It is important to note that while this method is specifically designed for structural damage quantification in this study, it may also be applicable to other similar inverse problems.

III. Validation of the Proposed Approach on Damaged Helicopter Panels

This section validates the proposed PDVNN and the damage quantification framework using a set of damaged aeronautical panels. Section III.A describes the panels and details the experimental setup and numerical model. Section III.B covers the construction of the simulated and experimental datasets used for training and validation of the PDVNN model. Section III.C explains the implementation of the method and the configuration of hyperparameters. Finally, Section III.D introduces two pure data-driven methods for comparison and outlines the performance evaluation metrics.

A. Helicopter Fuselage Panel and its Numerical Model

The aft fuselage of helicopters experiences substantial stresses, primarily due to torque resistance from the main and tail rotors. In this study, a set of helicopter fuselage panel specimens is used for validation. Each panel consists of a skin attached to stringers via rivets.

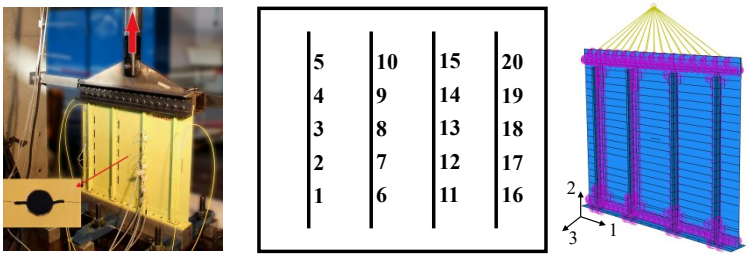

(a) (b) (c)

Fig. 7 Experiment and simulation of the fuselage panel. (a) Experiment setup; (b) Sensor positions and labels; (c) Numerical model.

The skin measures 600 mm in width, 500 mm in height, and 0.81 mm in thickness, and is fabricated from Al 2024-T6 alloy. The four L-shaped stringers, made of Al 7075-T76 alloy, are 435 mm in length and 1.2 mm in thickness and are evenly spaced over the specimen's skin surface. The fatigue crack growth tests were conducted as depicted in Fig. 7 (a). The specimen is equipped with 20 Fiber Bragg Grating (FBG) sensors, arranged along the rivet line to collect static strain at peak load, as shown in Fig. 7 (b). Initial response data is collected from an undamaged panel to establish a benchmark signal for model validation. Subsequently, an initial 16 mm of damage is artificially introduced at the center of the panel. The specimen is then subjected to sinusoidal loading with an amplitude of $F_{\max}$ = 35kN and a stress ratio of R = 0.1 [53].

The finite element model, implemented in ABAQUS, replicates the structural behavior depicted in Fig. 7 (c).

Quadratic shell elements (S9R5) are used to model the skin and stringers, while triaxial springs represent the rivets. Each stringer is connected to the skin via rivets [54].

B. Experimental and Simulated Dataset

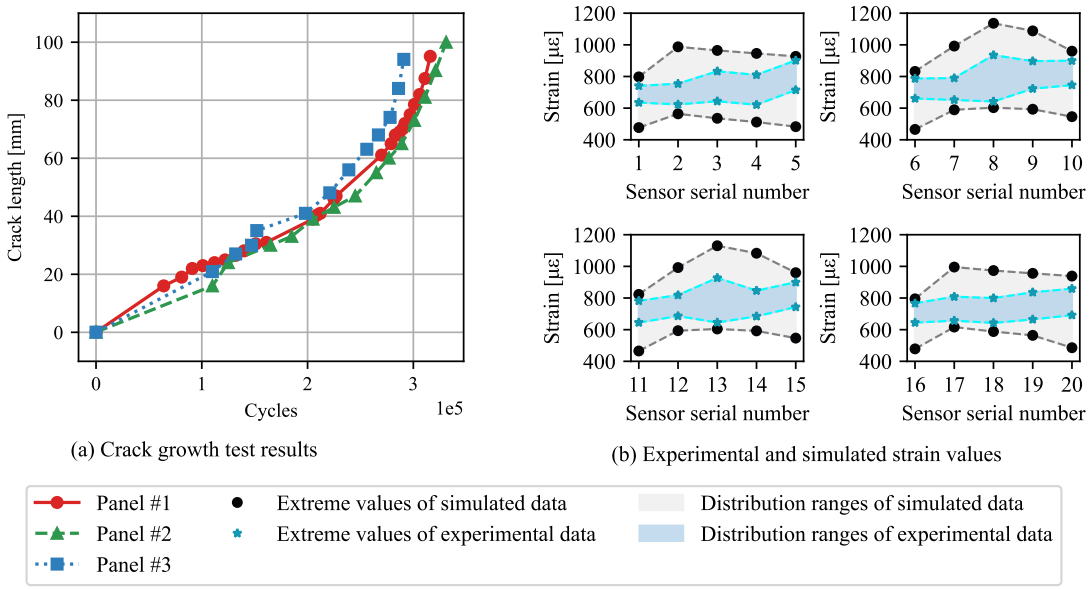

Fig. 8 (a) results of three crack growth experiment and (b) Experimental and simulated strain range of 20 FBG sensors.

In this study, simulated datasets are used to train the PDVNN model, while the experimental dataset are employed to validate its performance.

First, the experimental dataset is introduced. Crack growth data were collected from three stiffened panel specimens, labeled #1, #2, and #3. The crack growth histories of these panels are shown in Fig. 8 (a). Strain measurements from 20 FBG sensors and corresponding crack lengths were recorded, with 29, 15, and 13 measurements for each panel, respectively. To mitigate the impact of load variations on strain measurements during the fatigue crack growth, a damage index is defined based on the detected signals [55, 56]. Assuming N_s strain sensors are arranged along the rivet line to collect static strain at peak load, the damage index $\varepsilon_k^{\text{norm}}$ of the k_{th} sensor is defined as:

$$\varepsilon_k^{\text{norm}} = \frac{\varepsilon_k}{\sum_{i=1}^{N} \frac{\varepsilon_i}{N_s}} \tag{8}$$

Thus, the resulting experimental dataset is denoted as:

$$\mathcal{D}_{\text{panel}}^{\text{exp}} = \left\{ \mathbf{a}_i, \boldsymbol{\varepsilon}_i^{\text{norm}} \right\} \tag{9}$$

Table 1 Distribution range of influencing parameters

Parameter	Meaning	Nominal value	Range
t_{p}	Thickness of the skin	0.80 [mm]	0.74 ~ 0.82 [mm]
t_{s1}	Thickness of the first stringer	1.30 [mm]	1.0 ~ 1.3 [mm]
t_{s2}	Thickness of the second stringer	1.30 [mm]	1.0 ~ 1.3 [mm]
E_{p}	Young's modulus of the skin	73.8 [GPa]	71.5 ~ 74.5 [GPa]
E_{s1}	Young's modulus of the first stringer	70.3 [GPa]	69.0 ~ 72.0 [GPa]
E_{s2}	Young's modulus of the second stringer	70.3 [GPa]	69.0 ~ 72.0 [GPa]
μ_i	Weight of the i_{th} constraint mode	$[1, 0, 0]$	$\sum_3^{i=1} \mu_i = 1$ and $\mu_i > 0$

where $i = 1, 2, 3$ corresponds to the three crack growth experiments, $\mathbf{a}_i$ is the crack length set of the i_{th} panel, $\boldsymbol{\varepsilon}_i^{\mathrm{norm}}$ is the damage index set of the i_{th} panel.

Second, the simulated dataset is introduced. After evaluating the influence of various parameters on the simulation outputs, the geometric dimensions and material properties of the connectors on the upper and lower parts of the panels were fixed. Attributes closely related to structural damage, such as those of the skin and stringers, were identified as influencing parameters. The types and ranges of these parameters are detailed in Table 1.

For complex boundary constraints encountered in real service scenarios, state superposition is an effective method to characterize constraints by weighted averaging different constraint modes [57], the superposed simulated strain signal $\boldsymbol{\varepsilon}_{\mathrm{panel}}^{\mathrm{sim}}$, is calculated as follows:

$$\boldsymbol{\varepsilon}_{\mathrm{panel}}^{\mathrm{sim}} = \sum_{i=1}^{3} \mu_i \boldsymbol{\varepsilon}_i^{\mathrm{sim}} \quad \text{with} \quad \sum_{i=1}^{3} \mu_i = 1 \tag{10}$$

where μ_i represents the weight corresponding to the i_{th} constraint mode, $\boldsymbol{\varepsilon}_i^{\mathrm{sim}}$ is the simulated strain in a single constraint mode.

In this study, three constraint modes are considered for the panels, as detailed in Table 2. For all three modes, the degrees of freedom (DOFs) at the lower end of the panels are fixed. At the upper end, the constraints vary as follows: the first mode restricts both out-of-plane translation and rotation, consistent with the original model [55] the second mode permits only vertical translation, as referenced in [57]; and the third mode allows out-of-plane translation only, which is a relaxation compared to the first mode. It is important to note that the weighted sum of the three constraint modes equals 1, indicating that only two of the constraint modes are independent. Therefore, only the weights of the first two modes are utilized in the influencing parameters.

As a result, the final set of influencing parameters of the panel $\boldsymbol{\Lambda}_{\mathrm{panel}}^{\mathrm{sim}}$ consist of eight parameters as:

$$\boldsymbol{\Lambda}_{\mathrm{panel}}^{\mathrm{sim}} = \left\{ t_{\mathrm{p}}, t_{\mathrm{s1}}, t_{\mathrm{s2}}, E_{\mathrm{p}}, E_{\mathrm{s1}}, E_{\mathrm{s2}}, \mu_1, \mu_2 \right\} \tag{11}$$

Table 2 Constraints on the degrees of freedom (DOFs) at the clamping end for different constraint modes

Mode	Lower end DOFs	Upper end DOFs
1	$u_i = ur_i = 0, i = 1, 2, 3$	$u_3 = ur_1 = ur_2 = 0$
2	$u_i = ur_i = 0, i = 1, 2, 3$	$u_1 = u_3 = ur_i = 0, i = 1, 2, 3$
3	$u_i = ur_i = 0, i = 1, 2, 3$	$ur_1 = ur_2 = 0$

where μ_1 and μ_2 represents the weight corresponding to the first and second constraint mode, respectively.

The process for generating the simulated dataset for the helicopter fuselage panel structure is outlined as follows:

1) Latin Hypercube Sampling (LHS): LHS was employed to generate a sufficient number (in this study is 10000) of data points across the space of crack sizes $\mathbf{a}_{\text{panel}}^{\text{sim}}$ and influencing parameters $\mathbf{\Lambda}_{\text{panel}}^{\text{sim}}$, as detailed in Table 1, ensuring a statistically meaningful distribution of samples within the parameter space.
2) Parametric Modeling in ABAQUS: Crack sizes and influencing parameters were incorporated into script files using ABAQUS's parametric modeling capabilities, generating corresponding INP files for each sample point.
3) Automated Simulation Analysis: The ABAQUS solver was employed to perform automated simulations based on the structural models specified in the INP files. These simulations generated structural responses, and strains were extracted from 20 sensor locations.
4) Data Analysis: Outliers were eliminated from the simulation results, resulting in a final dataset comprising 9862 samples.

Thus, the resulting simulated dataset is denoted as:

$$\mathcal{D}_{\text{panel}}^{\text{sim}} = \left\{ \mathbf{a}_{\text{panel}}^{\text{sim}}, \mathbf{\Lambda}_{\text{panel}}^{\text{sim}}, \mathbf{x}_{\text{panel}}^{\text{sim}} \right\} \tag{12}$$

The range of simulated and measured strains is shown in Fig. 8 (b). It can be observed that the strain range of the simulated dataset $\mathcal{D}_{\text{panel}}^{\text{sim}}$ encompasses the strain range of the experimental dataset $\mathcal{D}_{\text{panel}}^{\text{exp}}$. This comprehensive coverage is crucial for parameter calibration, as it ensures that the calibration process relies primarily on interpolation rather than extrapolation. Such coverage enhances the stability and reliability of the calibration process.

C. Implementation of the PDVNN and Hyperparameter Setting

Using the simulated dataset $\mathcal{D}_{\text{panel}}^{\text{sim}}$, the PDVNN model for the damage quantification and parameter calibration of the panels are constructed.

Initially, the reduced-order digital twin model was pretrained with a neural network. The network's input size was 9, representing the combined number of damage state and influencing parameters, while the output size was 20, corresponding to the number of FBG sensors. This pretrained neural network consisted of two hidden layers, with 13

Table 3 PDVNN parameters applied to panel damage quantification

Parameter	Setting
Learning rate scheduler	Cosine learning rate from 0.05 to 0.0003
Epochs	5000
Batch size	64
Activation	Sigmoid

and 27 neurons, respectively.

Subsequently, this reduced-order digital twin was integrated into the PDVNN framework. The physical feature extraction model within the PDVNN also had two hidden layers but with 23 and 12 neurons, respectively. The input and output sizes of this model were reversed compared to the pretrained digital twin.

For training the PDVNN, the simulated dataset $\mathcal{D}^{\text{sim}}_{\text{panel}}$ is partitioned into training and validation subsets in an 0.8/0.2 ratio. The network was then optimized using the Adam optimizer, with specific hyperparameters detailed in Table 3. To prevent overfitting, early stopping is applied during training. The training and validation losses over the course of 5000 epochs are depicted in Fig. 9. The results indicate that the training loss generally remained lower than the validation loss, with the difference between them being within a reasonable range, suggesting effective model learning.

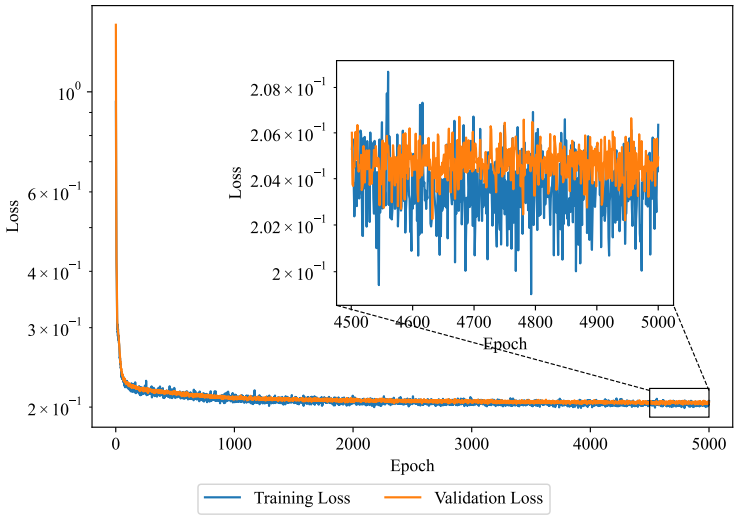

Fig. 9 Training process of the PDVNN.

D. Methods for Comparison and Performance Evaluation

This study compares the proposed PDVNN with two classical pure data-driven methods: Artificial Neural Network (ANN) and Random Forest (RF). Both methods were configured with parameter settings comparable to those used for the PDVNN, as illustrated in Fig. 10.

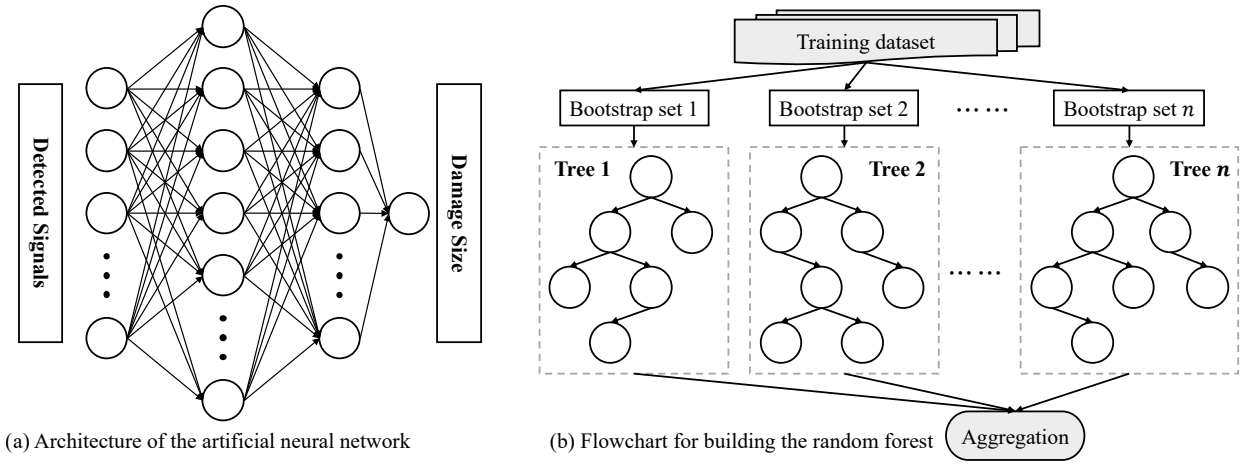

(a) Architecture of the artificial neural network

(b) Flowchart for building the random forest

Fig. 10 Illustration of (a) Artificial neural network and (b) Random forest.

Artificial Neural Network is commonly used to develop surrogate models that map detected signals to damage states. However, traditional ANN models neither incorporate physical mechanisms nor quantify uncertainty. The ANN architecture employed in this study consists of a fully connected layer with 29 × 17 neurons connected to the input layer, which processes the 20 FBG measurements, and an output layer with a single neuron representing the damage size. To account for the randomness inherent in initialization and training, 20 ANN models were trained, and their predictions were averaged to derive the result. The architecture of the ANN is shown in Fig. 10 (a).

Random Forest model consists of multiple decision trees, each functioning as an individual model. The RF model is constructed by randomly selecting subsets of variables and samples from the training dataset and using a deterministic algorithm to build the trees. For this study, two-thirds of the training dataset were used to develop the regression function, while the remaining one-third served as out-of-bag samples. The tuned RF model includes 100 trees, each with a depth of 10 layers and leaf nodes containing four samples. The flowchart for constructing a RF model is shown in Fig. 10 (b).

The accuracy of damage quantification is evaluated using the root mean square error (RMSE) metric, defined as follows:

$$\text{RMSE} = \sqrt{\frac{1}{n}\sum_{i=1}^{n}(y_i - \hat{y}_i)^2} \tag{13}$$

where y_i denotes the i_{th} measured value, $\hat{y}_i$ represents the i_{th} predicted value, and n is the number of samples.

During testing, predictions are generated for each sample, and the predicted damage values are compared to the measured damage lengths to compute the RMSE.

IV. Results and Discussion

In this section, the effectiveness of the proposed PDVNN for probabilistic damage quantification and parameter calibration is evaluated. The performance of PDVNN is compared with existing methods using experimental data from the helicopter fuselage panels. Section IV.A presents a comparative analysis of PDVNN against two classical data-driven methods, demonstrating its superior performance. Section IV.B illustrates the model's capability for parameter calibration, enabling individualized damage quantification across a fleet of similar structures. Finally, Section IV.C contrasts PDVNN with a simplified version that omits uncertainty considerations, highlighting the critical importance of incorporating uncertainty quantification in the proposed framework.

A. The Quantification Results of Structural Damage of PDVNN Compared with Data-Driven ANN and RF

In this subsection, the capability of PDVNN for structural damage quantification is validated using data from three experimental panels.

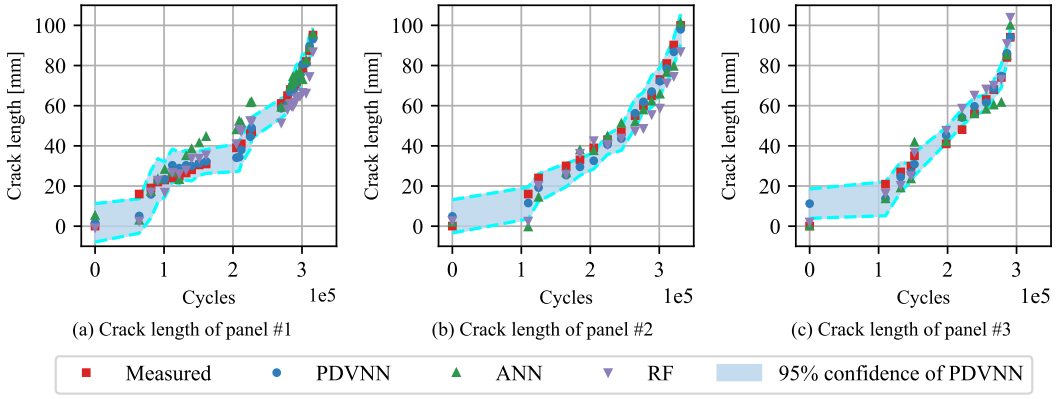

Fig. 11 Comparison of crack size quantification among PDVNN, ANN and RF.

Fig. 11 illustrates the crack size quantification based on detected FBG strains during the fatigue crack growth test, comparing results from PDVNN, ANN, and RF models. The ANN and RF models were trained with a simulated dataset consisting of 101 samples, where crack sizes were uniformly distributed from 0 mm to 100 mm, with geometric, material, and constraint parameters set to nominal values.

The measured crack lengths from all three panels align closely with the PDVNN predictions, generally falling within the 95% confidence intervals. As crack lengths increase during the fatigue crack growth, the uncertainties in the damage quantification performed by PDVNN progressively decrease. This reduction in uncertainty may be attributed to an increase in the signal-to-noise ratio of the strain signal as the crack size grows. In contrast, predictions from the ANN and RF models exhibit larger errors compared to those from PDVNN. This discrepancy is attributed to the limitations of purely data-driven methods, which fail to account for influencing parameters and thus struggle to address discrepancies between the simulation model and real structures. Fig. 12 compares quantification errors between PDVNN, ANN, and

RF. Over the entire damage process, the average RMSE for ANN and RF are 6.978 mm and 7.319 mm, respectively, whereas for PDVNN it is 4.652±1.870 mm. This indicates that PDVNN outperforms the pure data-driven methods represented by ANN and RF in terms of damage quantification accuracy.

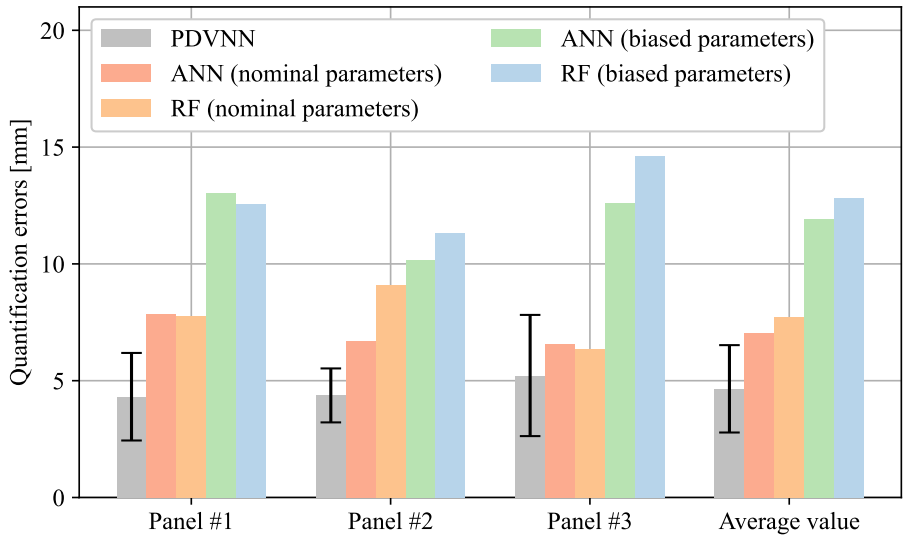

Fig. 12 Comparison of quantification errors among PDVNN and pure data-driven methods.

Since the ANN and RF models are trained using a simulated dataset, the parameters in the full-order simulation model significantly impact their performance. To illustrate this, additional ANN and RF models were trained using the same dataset and model settings but with minor changes to the skin thickness (from 0.80 mm to 0.78 mm) and Young's modulus of the skin (from 73.8 GPa to 74.0 GPa). As shown in Fig. 12, the performance of the ANN and RF models decreased significantly. This demonstrates that when the finite element model deviates from nominal values of influencing parameters and lacks proper calibration, the prediction results can significantly diverge from true values.

B. Validation of PDVNN for the Physical Feature Calibration

Fig. 13 and Fig. 14 illustrate the calibration results of influencing parameters across three panels, which have identical nominal dimensions and material properties. Variations in stringer and skin thicknesses, as well as Young's moduli from nominal values, are evident based on features extracted from detected signals. Fig. 15 depicts the calibration for boundary constraint modes across these panels. Notably, modes #2 and #3 exhibit significantly lower weights compared to mode #1, indicating that while panels experience complex constraints during testing, they align closely with the ideal constraint condition represented by mode #1.

These results highlight that PDVNN enhances the interpretability of damage quantification models through effective parameter calibration. The calibrated parameters enable the creation of more accurate digital twins, yielding simulation

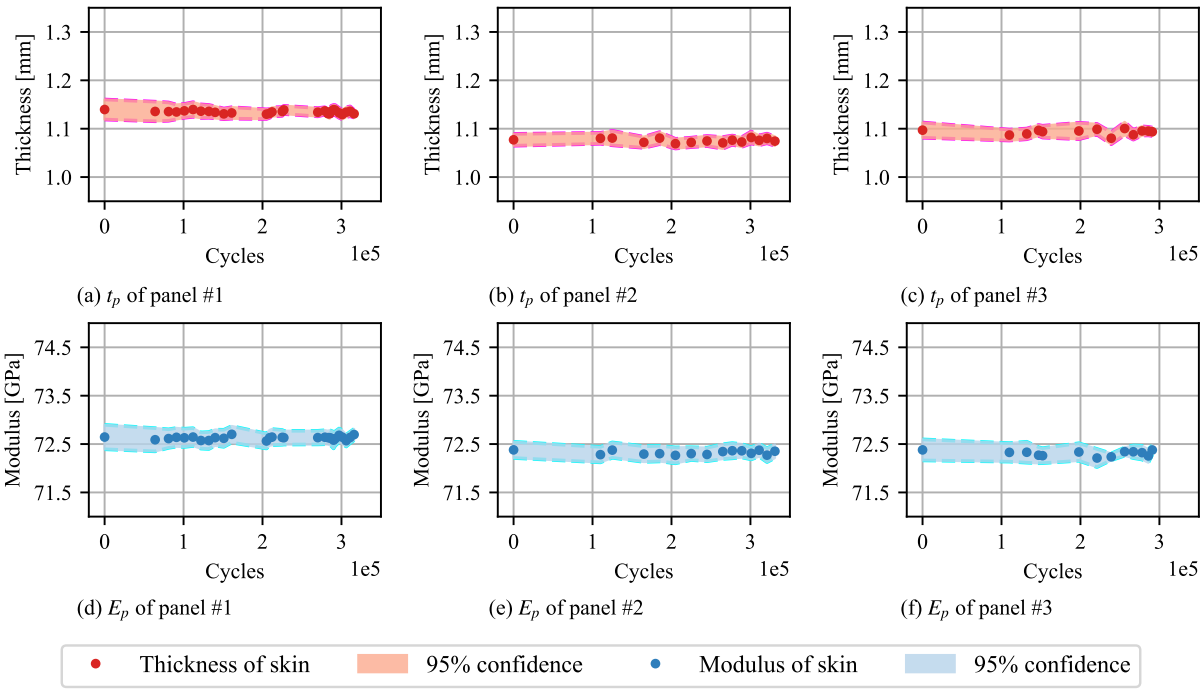

Fig. 13 Calibration of skin parameters by PDVNN.

outcomes that closely mirror realistic structural behaviors. Additionally, it would support individualized damage quantification for similar aircraft structures across the fleet, a capability that traditional feature extraction methods lacking embedded domain knowledge cannot provide.

C. Comparison with the Physics-Decoded Neural Network Omits Uncertainty Considerations

Given the inherent uncertainties in the real-world damage growth process, integrating these uncertainties into simulation models is crucial for accurate quantification. To illustrate this necessity, the PDVNN is compared with a simplified version that does not account for uncertainties, referred to as the Physics-Decoded Neural Network (PDNN). Although the PDNN also utilizes the reduced-order digital twin as the decoder, it relies on a deterministic training process, using only the reconstruction loss function without considering uncertainties in the physical features.

Fig. 16 illustrates the comparison of the damage quantification of PDVNN and PDNN based on the experimental dataset. It is evident that the PDNN exhibits greater variability, particularly when the structure is damaged. This variability likely arises from the absence of uncertainty modeling in PDNN, which makes it more susceptible to noise, thereby affecting the feature extraction process and reducing the accuracy of damage state estimation across different samples under the same damage conditions. Table 4 presents the prediction errors for both methods, highlighting significantly larger prediction errors for crack size with PDNN compared to PDVNN. These results underscore the importance of incorporating variational inference in PDVNN for effective uncertainty quantification.

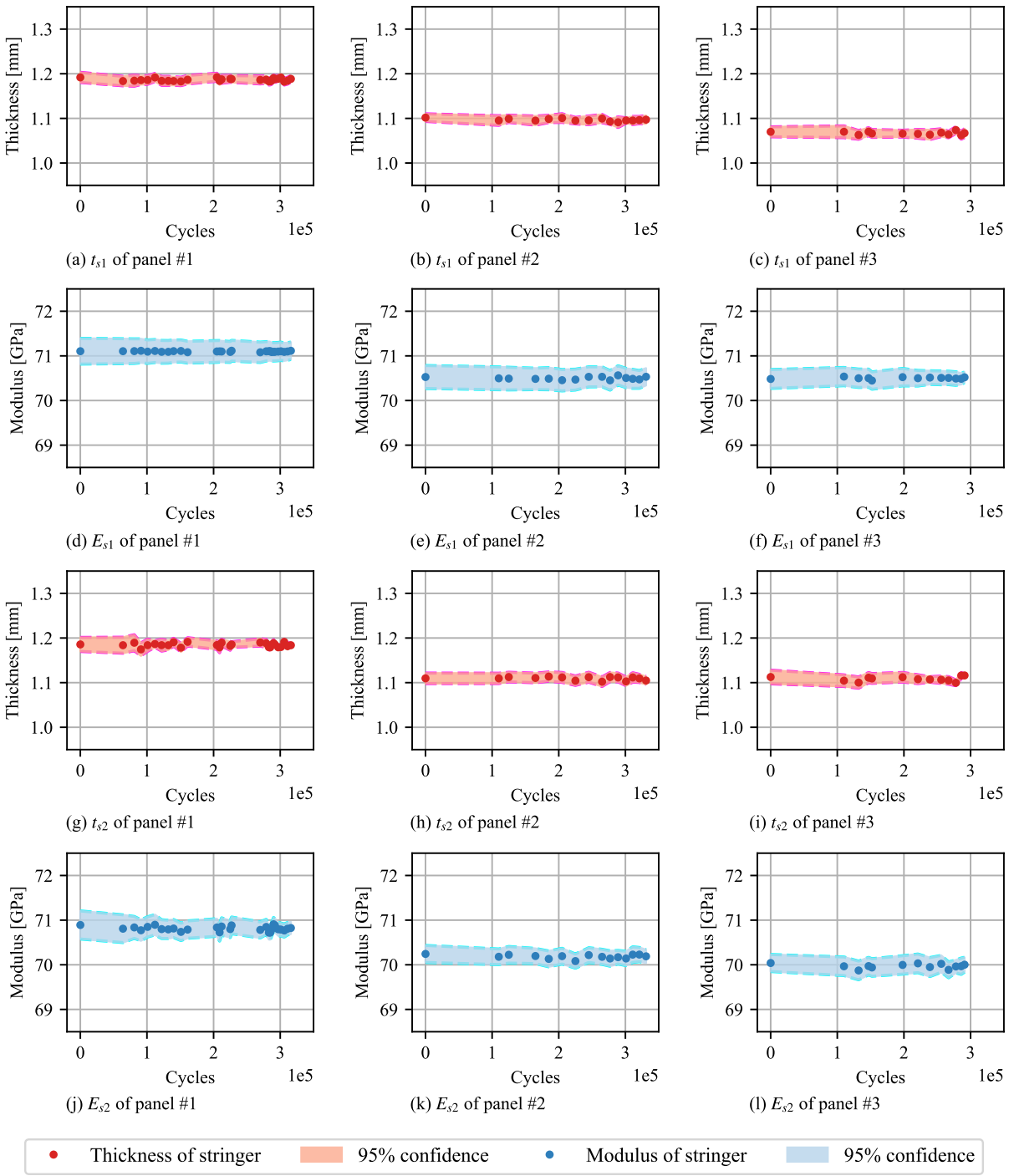

Fig. 14 Calibration of stringer parameters by PDVNN.

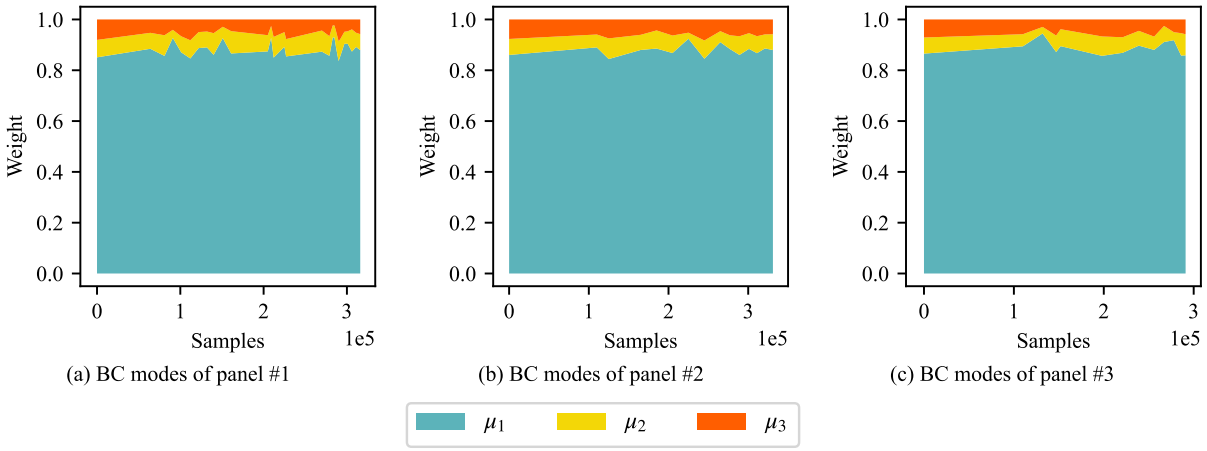

Fig. 15 Calibration of weights of boundary constraint modes by PDVNN.

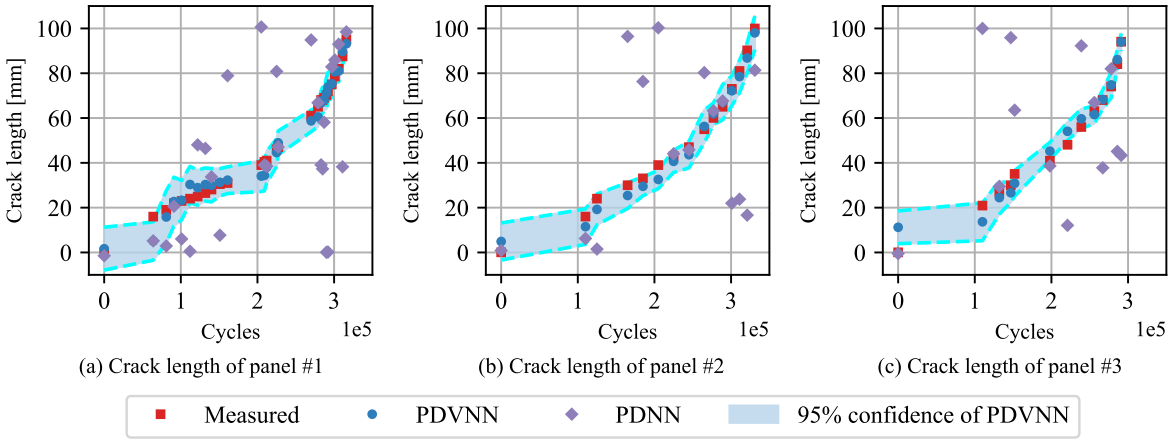

Fig. 16 Comparison of crack size quantifications between PDVNN and PDNN.

Table 4 Comparison of quantification errors between PDVNN and PDNN

Method	Prediction Error [mm]			
	Panel #1	Panel #2	Panel #3	Average value
PDVNN	4.314 ± 1.874	4.370 ± 1.155	5.222 ± 2.594	4.652 ± 1.870
PDNN	30.73	37.73	38.21	35.56

V. Conclusion

This study presents a novel approach that integrates a reduced-order digital twin into a variational neural network, referred to as the Physics-Decoded Variational Neural Network (PDVNN). This integrated framework offers a promising solution for online probabilistic damage quantification and parameter calibration in aeronautical structures. The practical implementation of this method begins with the development of a reduced-order digital twin, which incorporates both damaged and influencing parameters as physical features. By embedding domain knowledge within the digital twin, the physical feature extraction model is effectively constrained and guided during training. Through variational inference, the model successfully quantifies structural damage states based on detected signals and calibrates the digital twin's parameters within an uncertainty framework.

Experimental results on typical aeronautical panels validate the efficacy of the PDVNN for online probabilistic structural damage quantification and digital twin model parameter calibration. Comparative analysis with pure data-driven methods, such as ANN and RF, highlights the superior performance of the proposed method in both the accuracy of damage quantification and the confidence in the results. Notably, although the PDVNN model is trained with a simulated dataset, it performs well with experimental data. Additionally, comparisons with PDNN emphasize the critical importance of incorporating uncertainty quantification into the physical decoding process, underscoring the necessity of variational inference to ensure stability in feature extraction.

This study marks an initial exploration of applying PDVNN to structural damage state quantification, establishing a flexible framework capable of individualized damage assessment for structures across different aircraft within a fleet. The framework's adaptability makes it suitable for integration into airframe digital twin systems for condition-based maintenance. Moreover, it offers a valuable reference for research in other fields, paving the way for the development of reduced-order digital twins combined with domain-specific knowledge to tackle inverse problems across diverse applications.

Acknowledgments

The work of the first two authors and the fifth author was supported by the National Natural Science Foundation of China (Grant Nos. 52402510, 12072011), the Aeronautical Science Foundation of China (Grant No. 201909051001), and the "111 Center" (Program No. B18002). The second author was supported by the Postdoctoral Fellowship Program of China Postdoctoral Science Foundation (Grant No. GZB20240931).

References

[1] Zhang, Z., Mao, H., Liu, Y., Jiao, P., Hu, W., and Shen, P., "A Risk Assessment Method of Aircraft Structure Damage Maintenance Interval Indexed by: Considering Fatigue Crack Growth and Detection Rate," *Eksploatacja i Niezawodność – Maintenance and Reliability*, Vol. 25, No. 1, 2023, pp. 24–34. https://doi.org/10.17531/ein.2023.1.3.

[2] Guratzsch, R. F., and Mahadevan, S., "Structural Health Monitoring Sensor Placement Optimization Under Uncertainty," *AIAA Journal*, Vol. 48, No. 7, 2010, pp. 1281–1289. https://doi.org/10.2514/1.28435.

[3] Liu, Y., Wang, L., and Ng, B. F., "Load-Independent Multi-Objective Sensor Placement Method for Localization and Reconstruction of External Excitations under Interval Uncertainties," *Computer Methods in Applied Mechanics and Engineering*, Vol. 416, 2023, p. 116344. https://doi.org/10.1016/j.cma.2023.116344.

[4] Sbarufatti, C., "Optimization of an Artificial Neural Network for Fatigue Damage Identification Using Analysis of Variance," *Structural Control and Health Monitoring*, Vol. 24, No. 9, 2017, p. e1964. https://doi.org/10.1002/stc.1964.

[5] Galea, S. C., and Rajic, N., "Development and Validation Roadmap for *In Situ* Structural Health Monitoring of ADF Aircraft," *Key Engineering Materials*, Vol. 558, 2013, pp. 534–545. https://doi.org/10.4028/www.scientific.net/KEM.558.534.

[6] Ewald, V., Sridaran Venkat, R., Asokkumar, A., Benedictus, R., Boller, C., and Groves, R. M., "Perception Modelling by Invariant Representation of Deep Learning for Automated Structural Diagnostic in Aircraft Maintenance: A Study Case Using DeepSHM," *Mechanical Systems and Signal Processing*, Vol. 165, 2022, p. 108153. https://doi.org/10.1016/j.ymssp.2021.108153.

[7] Farrar, C. R., and Worden, K., *Structural Health Monitoring: A Machine Learning Perspective*, Wiley, Chichester, West Sussex, U.K. ; Hoboken, N.J, 2013.

[8] Parziale, M., Lomazzi, L., Giglio, M., and Cadini, F., "Physics-Informed Neural Networks for the Condition Monitoring of Rotating Shafts," *Sensors*, Vol. 24, No. 1, 2023, p. 207. https://doi.org/10.3390/s24010207.

[9] Lomazzi, L., Junges, R., Giglio, M., and Cadini, F., "Unsupervised Data-Driven Method for Damage Localization Using Guided Waves," *Mechanical Systems and Signal Processing*, Vol. 208, 2024, p. 111038. https://doi.org/10.1016/j.ymssp.2023.111038.

[10] Yuan, S., Jing, H., Wang, Y., and Zhang, J., "A Whole Service Time SHM Damage Quantification Model Hierarchical Evolution Mechanism," *Mechanical Systems and Signal Processing*, Vol. 209, 2024, p. 111064. https://doi.org/10.1016/j.ymssp.2023.111064.

[11] Shao, W., Sun, H., Zhou, Q., Wang, Y., and Qing, X., "A Novel Lamb Wave-Based Multi-Damage Dataset Construction and Quantification Algorithm under the Framework of Multi-Task Deep Learning," *Structural Health Monitoring*, Vol. 23, No. 2, 2024, pp. 1148–1169. https://doi.org/10.1177/14759217231185051.

[12] Xiao, D., Sharif-Khodaei, Z., and Aliabadi, M., "Hybrid Physics-Based and Data-Driven Impact Localization for Composite Laminates," *International Journal of Mechanical Sciences*, Vol. 274, 2024, p. 109222. https://doi.org/10.1016/j.ijmecsci.2024.109222.

[13] Moradi, M., "A Novel Machine Learning Model to Design Historical-Independent Health Indicators for Composite Structures," *Composites Part B*, Vol. 275, 2024, p. 111328. https://doi.org/10.1016/j.compositesb.2024.111328.

[14] Giglioni, V., Poole, J., Venanzi, I., Ubertini, F., and Worden, K., "A Domain Adaptation Approach to Damage Classification with an Application to Bridge Monitoring," *Mechanical Systems and Signal Processing*, Vol. 209, 2024, p. 111135. https://doi.org/10.1016/j.ymssp.2024.111135.

[15] Azimi, M., Eslamlou, A., and Pekcan, G., "Data-Driven Structural Health Monitoring and Damage Detection through Deep Learning: State-of-the-Art Review," *Sensors*, Vol. 20, No. 10, 2020, p. 2778. https://doi.org/10.3390/s20102778.

[16] Chen, R., Wang, S., Zhang, C., Dui, H., Zhang, Y., Zhang, Y., and Li, Y., "Component Uncertainty Importance Measure in Complex Multi-State System Considering Epistemic Uncertainties," *Chinese Journal of Aeronautics*, 2024, p. S1000936124001912. https://doi.org/10.1016/j.cja.2024.05.024.

[17] Eltouny, K., Gomaa, M., and Liang, X., "Unsupervised Learning Methods for Data-Driven Vibration-Based Structural Health Monitoring: A Review," *Sensors*, Vol. 23, No. 6, 2023, p. 3290. https://doi.org/10.3390/s23063290.

[18] Chen, Y., Huang, D., Zhang, D., Zeng, J., Wang, N., Zhang, H., and Yan, J., "Theory-Guided Hard Constraint Projection (HCP): A Knowledge-Based Data-Driven Scientific Machine Learning Method," *Journal of Computational Physics*, Vol. 445, 2021, p. 110624. https://doi.org/10.1016/j.jcp.2021.110624.

[19] Faroughi, S. A., Pawar, N. M., Fernandes, C., Raissi, M., Das, S., Kalantari, N. K., and Kourosh Mahjour, S., "Physics-Guided, Physics-Informed, and Physics-Encoded Neural Networks and Operators in Scientific Computing: Fluid and Solid Mechanics," *Journal of Computing and Information Science in Engineering*, Vol. 24, No. 4, 2024, p. 040802. https://doi.org/10.1115/1.4064449.

[20] Neerukatti, R. K., Liu, K. C., Kovvali, N., and Chattopadhyay, A., "Fatigue Life Prediction Using Hybrid Prognosis for Structural Health Monitoring," *Journal of Aerospace Information Systems*, Vol. 11, No. 4, 2014, pp. 211–232. https://doi.org/10.2514/1.I010094.

[21] Figueiredo, E., Moldovan, I., Santos, A., and Campos, P., "Finite Element–Based Machine-Learning Approach to Detect Damage in Bridges under Operational and Environmental Variations," *J. Bridge Eng.*, Vol. 24, No. 7, 2019, p. 04019061. https://doi.org/10.1061/(ASCE)BE.1943-5592.0001432.

[22] Xu, R., Zhang, D., Rong, M., and Wang, N., "Weak Form Theory-Guided Neural Network (TgNN-wf) for Deep Learning of Subsurface Single- and Two-Phase Flow," *Journal of Computational Physics*, Vol. 436, 2021, p. 110318. https://doi.org/10.1016/j.jcp.2021.110318.

[23] Jian, X., Xia, Y., Duthé, G., Bacsa, K., Liu, W., and Chatzi, E., "Using Graph Neural Networks and Frequency Domain Data for Automated Operational Modal Analysis of Populations of Structures," , Jul. 2024.

[24] Shen, S., Lu, H., Sadoughi, M., Hu, C., Nemani, V., Thelen, A., Webster, K., Darr, M., Sidon, J., and Kenny, S., "A Physics-Informed Deep Learning Approach for Bearing Fault Detection," *Engineering Applications of Artificial Intelligence*, Vol. 103, 2021, p. 104295. https://doi.org/10.1016/j.engappai.2021.104295.

[25] Gao, C., Shi, Z., and Zhang, W., "Data-Knowledge-Driven Semi-Empirical Model Augmentation Method for Nonlinear Vortex-Induced Vibration," *Nonlinear Dynamics*, Vol. 111, No. 22, 2023, pp. 20617–20642. https://doi.org/10.1007/s11071-023-08966-x.

[26] Zhang, W., Peng, X., Kou, J., and Wang, X., "Heterogeneous Data-Driven Aerodynamic Modeling Based on Physical Feature Embedding," *Chinese Journal of Aeronautics*, Vol. 37, No. 3, 2024, pp. 1–6. https://doi.org/10.1016/j.cja.2023.11.010.

[27] Dourado, A., and Viana, F. A. C., "Physics-Informed Neural Networks for Corrosion-Fatigue Prognosis," *Annual Conference of the PHM Society*, Vol. 11, No. 1, 2019. https://doi.org/10.36001/phmconf.2019.v11i1.814.

[28] Sun, D., Li, Y., Liu, Z., Jia, S., and Noman, K., "Physics-Inspired Multimodal Machine Learning for Adaptive Correlation Fusion Based Rotating Machinery Fault Diagnosis," *Information Fusion*, Vol. 108, 2024, p. 102394. https://doi.org/10.1016/j.inffus.2024.102394.

[29] Xu, W., Zhou, Z., Li, T., Sun, C., Chen, X., and Yan, R., "Physics-Constraint Variational Neural Network for Wear State Assessment of External Gear Pump," *IEEE Transactions on Neural Networks and Learning Systems*, Vol. 35, No. 5, 2024, pp. 5996–6006. https://doi.org/10.1109/TNNLS.2022.3213009.

[30] Gao, S., Yu, Z., Zhang, Z., Feng, C., Yan, T., He, B., and Zio, E., "Physical Model Embedding-Based Generative Adversarial Networks for Unsupervised Fault Detection of Underwater Thrusters," *Ocean Engineering*, Vol. 298, 2024, p. 117190. https://doi.org/10.1016/j.oceaneng.2024.117190.

[31] Shukla, K., Di Leoni, P. C., Blackshire, J., Sparkman, D., and Karniadakis, G. E., "Physics-Informed Neural Network for Ultrasound Nondestructive Quantification of Surface Breaking Cracks," *Journal of Nondestructive Evaluation*, Vol. 39, No. 3, 2020, p. 61. https://doi.org/10.1007/s10921-020-00705-1.

[32] Khatir, S., Tiachacht, S., Le Thanh, C., Ghandourah, E., Mirjalili, S., and Abdel Wahab, M., "An Improved Artificial Neural Network Using Arithmetic Optimization Algorithm for Damage Assessment in FGM Composite Plates," *Composite Structures*, Vol. 273, 2021, p. 114287. https://doi.org/10.1016/j.compstruct.2021.114287.

[33] Rautela, M., and Gopalakrishnan, S., "Ultrasonic Guided Wave Based Structural Damage Detection and Localization Using Model Assisted Convolutional and Recurrent Neural Networks," *Expert Systems with Applications*, Vol. 167, 2021, p. 114189. https://doi.org/10.1016/j.eswa.2020.114189.

[34] Sun, H., Peng, L., Lin, J., Wang, S., Zhao, W., and Huang, S., "Microcrack Defect Quantification Using a Focusing High-Order SH Guided Wave EMAT: The Physics-Informed Deep Neural Network GuwNet," *IEEE Transactions on Industrial Informatics*, Vol. 18, No. 5, 2022, pp. 3235–3247. https://doi.org/10.1109/TII.2021.3105537.

[35] Cury, A., Ribeiro, D., Ubertini, F., and Todd, M. D. (eds.), *Structural Health Monitoring Based on Data Science Techniques*, Structural Integrity, Vol. 21, Springer International Publishing, Cham, 2022. https://doi.org/10.1007/978-3-030-81716-9.

[36] Zhang, Z., and Sun, C., "Structural Damage Identification via Physics-Guided Machine Learning: A Methodology Integrating Pattern Recognition with Finite Element Model Updating," *Structural Health Monitoring*, Vol. 20, No. 4, 2021, pp. 1675–1688. https://doi.org/10.1177/1475921720927488.

[37] Wang, R., Li, J., Li, L., An, S., Ezard, B., Li, Q., and Hao, H., "Structural Damage Identification by Using Physics-Guided Residual Neural Networks," *Engineering Structures*, Vol. 318, 2024, p. 118703. https://doi.org/10.1016/j.engstruct.2024.118703.

[38] Ye, Y., Yang, Q., Yang, F., Huo, Y., and Meng, S., "Digital Twin for the Structural Health Management of Reusable Spacecraft: A Case Study," *Engineering Fracture Mechanics*, Vol. 234, 2020, p. 107076. https://doi.org/10.1016/j.engfracmech.2020.107076.

[39] Ye, Y., Yang, Q., Zhang, J., Meng, S., and Wang, J., "A Dynamic Data Driven Reliability Prognosis Method for Structural Digital Twin and Experimental Validation," *Reliability Engineering & System Safety*, Vol. 240, 2023, p. 109543. https://doi.org/10.1016/j.ress.2023.109543.

[40] Miele, S., Karve, P., and Mahadevan, S., "Multi-Fidelity Physics-Informed Machine Learning for Probabilistic Damage Diagnosis," *Reliability Engineering & System Safety*, Vol. 235, 2023, p. 109243. https://doi.org/10.1016/j.ress.2023.109243.

[41] Zhao, F., Zhou, X., He, S., Wang, C., Dong, L., and Atluri, S. N., "B-Spline Surface-Based Reduced-Order Modeling of Nonplanar Crack Growth in Structural Digital Twins," *AIAA Journal*, Vol. 62, No. 1, 2024, pp. 360–373. https://doi.org/10.2514/1.J062959.

[42] Zhou, X., Sbarufatti, C., Giglio, M., Dong, L., and Atluri, S., "Copula-Based Collaborative Multistructure Damage Diagnosis and Prognosis for Fleet Maintenance Digital Twins," *AIAA Journal*, Vol. 61, 2023, pp. 4735–4740. https://doi.org/10.2514/1.J063105.

[43] Zhou, X., He, S., Dong, L., and Atluri, S. N., "Real-Time Prediction of Probabilistic Crack Growth with a Helicopter Component Digital Twin," *AIAA Journal*, Vol. 60, No. 4, 2022, pp. 2555–2567. https://doi.org/10.2514/1.J060890.

[44] Dai, J., Liu, P., Li, L., Qu, Q., and Niu, T., "Multi-Disciplinary and Multi-Objective Optimization Method Based on Machine Learning," *AIAA Journal*, Vol. 62, No. 2, 2024, pp. 691–707. https://doi.org/10.2514/1.J063213.

[45] Anhichem, M., Timme, S., Castagna, J., Peace, A. J., and Maina, M., "Data Fusion of Wing Pressure Distributions Using Scalable Gaussian Processes," *AIAA Journal*, Vol. 62, No. 5, 2024, pp. 1946–1961. https://doi.org/10.2514/1.J063317.

[46] Li, Z., Liu, F., Yang, W., Peng, S., and Zhou, J., "A Survey of Convolutional Neural Networks: Analysis, Applications, and Prospects," *IEEE Transactions on Neural Networks and Learning Systems*, Vol. 33, No. 12, 2022, pp. 6999–7019. https://doi.org/10.1109/TNNLS.2021.3084827.

[47] Sherstinsky, A., "Fundamentals of Recurrent Neural Network (RNN) and Long Short-Term Memory (LSTM) Network," *Physica D: Nonlinear Phenomena*, Vol. 404, 2020, p. 132306. https://doi.org/10.1016/j.physd.2019.132306.

[48] Wu, Z., Pan, S., Chen, F., Long, G., Zhang, C., and Yu, P. S., "A Comprehensive Survey on Graph Neural Networks," *IEEE Transactions on Neural Networks and Learning Systems*, Vol. 32, No. 1, 2021, pp. 4–24. https://doi.org/10.1109/TNNLS.2020.2978386.

[49] Mohseni, S.-R., Zeitouni, M. J., Parvaresh, A., Abrazeh, S., Gheisarnejad, M., and Khooban, M.-H., "FMI Real-Time Co-Simulation-Based Machine Deep Learning Control of HVAC Systems in Smart Buildings: Digital-twins Technology," *Transactions of the Institute of Measurement and Control*, Vol. 45, No. 4, 2023, pp. 661–673. https://doi.org/10.1177/01423312221119635.

[50] Kingma, D. P., and Welling, M., "Auto-Encoding Variational Bayes," , Dec. 2022. https://doi.org/10.48550/arXiv.1312.6114.

[51] LeCun, Y., Bengio, Y., and Hinton, G., "Deep Learning," *Nature*, Vol. 521, No. 7553, 2015, pp. 436–444. https://doi.org/10.1038/nature14539.

[52] Doersch, C., "Tutorial on Variational Autoencoders," , Jun. 2016. https://doi.org/10.48550/arXiv.1606.05908.

[53] Colombo, D., Giglio, M., and Manes, A., "3D Fatigue Crack Propagation Analysis of a Helicopter Component," *International Journal of Materials and Product Technology*, Vol. 30, No. 1/2/3, 2007, pp. 107–123. https://doi.org/10.1504/IJMPT.2007.013116.

[54] Sbarufatti, C., Manes, A., and Giglio, M., "Application of Sensor Technologies for Local and Distributed Structural Health Monitoring: APPLICATION OF SENSOR TECHNOLOGIES FOR LOCAL AND DISTRIBUTED SHM," *Structural Control and Health Monitoring*, Vol. 21, No. 7, 2014, pp. 1057–1083. https://doi.org/10.1002/stc.1632.

[55] Sbarufatti, C., Manes, A., and Giglio, M., "Performance Optimization of a Diagnostic System Based upon a Simulated Strain Field for Fatigue Damage Characterization," *Mechanical Systems and Signal Processing*, Vol. 40, No. 2, 2013, pp. 667–690. https://doi.org/10.1016/j.ymssp.2013.06.003.

[56] Zhou, X., Sbarufatti, C., Giglio, M., and Dong, L., "A Fuzzy-Set-Based Joint Distribution Adaptation Method for Regression and Its Application to Online Damage Quantification for Structural Digital Twin," *Mechanical Systems and Signal Processing*, Vol. 191, 2023, p. 110164. https://doi.org/10.1016/j.ymssp.2023.110164.

[57] Colombo, L., Oboe, D., Sbarufatti, C., Cadini, F., Russo, S., and Giglio, M., "Shape Sensing and Damage Identification with iFEM on a Composite Structure Subjected to Impact Damage and Non-Trivial Boundary Conditions," *Mechanical Systems and Signal Processing*, Vol. 148, 2021, p. 107163. https://doi.org/10.1016/j.ymssp.2020.107163.